

# Ca<sup>2+</sup>-store-dependent and -independent reversal of Stim1 localization and function

Jeremy T. Smyth, Wayne I. DeHaven, Gary S. Bird and James W. Putney, Jr\*

Laboratory of Signal Transduction, National Institute of Environmental Health Sciences, National Institutes of Health, Department of Health and Human Services, PO Box 12233, Research Triangle Park, NC 27709, USA

\*Author for correspondence (e-mail: putney@niehs.nih.gov)

Accepted 13 December 2007

*J. Cell Sci.* 121, 762-772 Published by The Company of Biologists 2008  
doi:10.1242/jcs.023903

## Summary

**Stim1 responds to depletion of ER Ca<sup>2+</sup> stores by rearranging from tubular structures throughout the ER into punctate structures near the plasma membrane, where it activates Orai store-operated Ca<sup>2+</sup> entry (SOCE) channels. However, the mechanism and structural determinants of the localization and reversal of Stim1 puncta formation are poorly understood. Using HEK293 cells expressing Stim1 tagged with enhanced yellow fluorescent protein (EYFP-Stim1), we show that the basis for SOCE termination is the reversal of the punctate Stim1 localization, which absolutely depends on SOCE-dependent store refilling. We also describe rapid, store-independent reversal of EYFP-Stim1 punctae by the ML-9 inhibitor of myosin-light-chain kinase (MLCK). ML-9 similarly inhibited SOCE and the Ca<sup>2+</sup>-release-activated Ca<sup>2+</sup> (CRAC) current. Reversal by ML-9 resulted in full re-establishment of the**

**tubular EYFP-Stim1 localization. A constitutively active EF-hand mutant of EYFP-Stim1 was also reversed by ML-9, regardless of the Ca<sup>2+</sup> store content. Inhibition by ML-9 was not due to MLCK inhibition as other inhibitors of MLCK had no effect. Finally, we provide evidence that EYFP-Stim1 punctae form in specific predetermined cellular loci. We conclude that SOCE is tightly coupled to formation of Stim1 puncta, and both SOCE and puncta formation involve a dynamic, reversible signaling complex that probably consists of components in addition to Stim1 and Orai channels.**

Supplementary material available online at  
<http://jcs.biologists.org/cgi/content/full/121/6/762/DC1>

Key words: Stim1, ML-9, Inhibitors, Store-operated channels

## Introduction

Store-operated Ca<sup>2+</sup> entry (SOCE) is initiated when intracellular stores, located in the endoplasmic reticulum (ER) or a specialized component of it, release their stored Ca<sup>2+</sup> and become depleted (Parekh and Putney, Jr, 2005; Smyth et al., 2006). ER Ca<sup>2+</sup> stores can become depleted physiologically as a consequence of signaling mechanisms, such as those involving G-protein-coupled or tyrosine kinase receptors, that result in activation of inositol (1,4,5)-trisphosphate receptors [Ins(1,4,5)P<sub>3</sub>Rs], which are intracellular Ca<sup>2+</sup> release channels located in the ER membrane. Ca<sup>2+</sup> that enters the cell by means of SOCE can enter the ER and replenish the intracellular stores by means of sarco/endoplasmic reticulum Ca<sup>2+</sup>-ATPase (SERCA) pumps located in the ER membrane. Thus, SOCE is important for re-establishing Ca<sup>2+</sup> store content to maintain physiological ER function as well as to maintain a readily releasable pool of Ca<sup>2+</sup>, which acts as an important second messenger in a variety of cellular functions.

It is now known that SOCE involves an orchestration of signaling molecules in the ER and the plasma membrane (PM) (Smyth et al., 2006). Stromal interaction molecule 1 (Stim1) resides in the membrane of the ER and has an EF-hand domain that extends into the ER lumen (Dziadek and Johnstone, 2007); this luminal EF-hand allows Stim1 to sense decreases in ER Ca<sup>2+</sup> content (Stathopoulos et al., 2006). Under conditions of full ER Ca<sup>2+</sup> stores, Stim1 is localized throughout the ER network in structures organized by the microtubule network (Smyth et al., 2007), but, when Ca<sup>2+</sup> stores are depleted, Stim1 rearranges into punctate structures close to the PM while still remaining in the ER membrane (Liou et al., 2005; Zhang et al., 2005; Mercer et al., 2006). Stim1 then in some

manner activates members of the Orai family (Orai1, Orai2 and Orai3) of SOCE channels, resulting in Ca<sup>2+</sup> entry into the cell (Feske et al., 2006; Vig et al., 2006; Zhang et al., 2006; Mercer et al., 2006; Soboloff et al., 2006).

Fundamental to the physiological role of SOCE is the fact that the process must be reversible. Thus, as Ca<sup>2+</sup> stores are refilled, SOCE should shut down to prevent Ca<sup>2+</sup> overload of the cell. In turn, the near-PM localization of Stim1 that occurs as a result of store depletion should also be reversed by store refilling to terminate Orai-mediated Ca<sup>2+</sup> entry. Here, we investigate and compare the physiological process of Stim1 reversal that rigorously depends upon Ca<sup>2+</sup> store content and a novel pharmacological reversal process that is independent of Ca<sup>2+</sup> store content. In addition, we demonstrate that the localization of Stim1 puncta is not a random process, but appears to be predetermined by unknown molecular and structural elements.

## Results

### Reversal of EYFP-Stim1 localization by store refilling through SOC channels

We have investigated the reversibility of the store depletion-induced rearrangement of EYFP-Stim1 into near-PM punctae by simultaneous measurements of total internal reflectance microscopy (TIRFM) and intracellular Ca<sup>2+</sup> concentrations. For these experiments, cells were co-transfected with plasmids encoding EYFP-Stim1 and the m5 muscarinic receptor. As shown in Fig. 1A, treatment of these cells with 300 μM carbachol in the presence of nominal extracellular Ca<sup>2+</sup> caused a rapid increase in intracellular Ca<sup>2+</sup> concentration due to Ca<sup>2+</sup> release, which was quickly followed

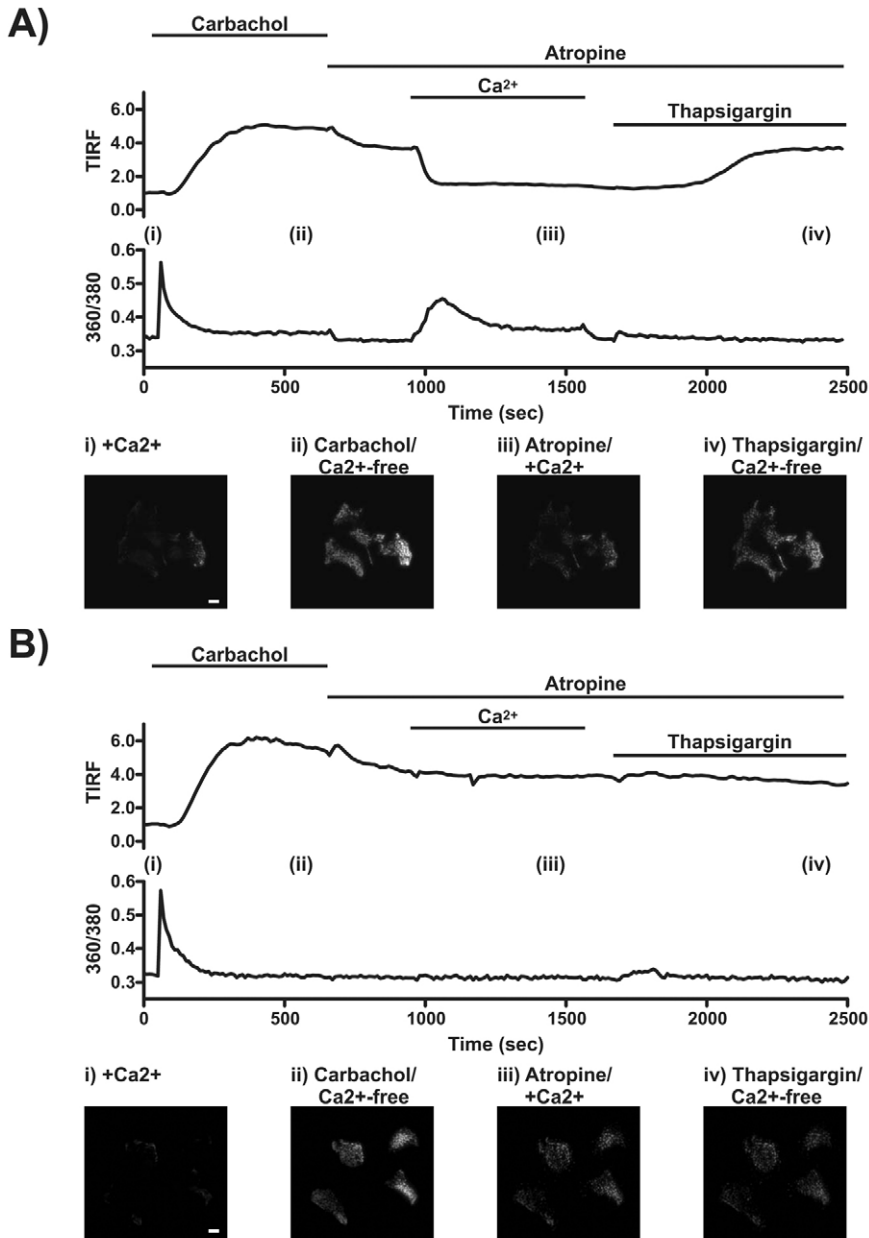


**Fig. 1.** Ca<sup>2+</sup> store refilling reverses the rearrangement of EYFP-Stim1. (A,B) TIRFM fluorescence intensity and relative intracellular Ca<sup>2+</sup> concentrations were measured simultaneously in the same HEK293 cells overexpressing EYFP-Stim1 and the m5 muscarinic receptor. As indicated, cells were treated with 300 μM carbachol in nominally Ca<sup>2+</sup>-free extracellular medium to deplete intracellular Ca<sup>2+</sup> stores. Carbachol signaling was then terminated by the addition of 50 μM atropine, after which extracellular Ca<sup>2+</sup> was restored to 1.8 mM. Fifteen minutes later, the cells were treated with 2 μM thapsigargin to demonstrate that store refilling had occurred. This protocol was performed with cells treated in the absence (A) or presence (B) of 5 μM Gd<sup>3+</sup> throughout. Note that in panel B SOCE did not occur upon restoration of extracellular Ca<sup>2+</sup>, and EYFP-Stim1 was not reversed. The upper traces show the TIRFM intensity profiles, and the bottom traces show the 360/380 fluorescence intensities representative of relative Ca<sup>2+</sup> responses; each trace represents the average response of four cells measured in a single experiment. The bottom panels show TIRFM images taken at the times indicated (i-iv) in the intensity profiles. Bars, 10 μm.

by an increase in TIRFM fluorescence intensity due to rearrangement of EYFP-Stim1 into near-PM punctae. The addition of 50 μM atropine to terminate carbachol signaling caused a small drop in both the Ca<sup>2+</sup> and TIRFM signals, probably owing to the presence of residual Ca<sup>2+</sup> in the nominally Ca<sup>2+</sup>-free extracellular

solution (~10 μM). Importantly, restoration of extracellular Ca<sup>2+</sup> to 1.8 mM caused a large increase in the intracellular Ca<sup>2+</sup> concentration as a result of SOCE, and this was accompanied simultaneously by a rapid decrease in the TIRFM signal. A similar dependence on extracellular Ca<sup>2+</sup> for reversal of Stim1 localization was reported by Varnai et al. (Varnai et al., 2007). This decrease in the near-PM localization of EYFP-Stim1 can be attributed to Ca<sup>2+</sup> store refilling by SOCE; when the identical experiment was performed in the presence of 5 μM Gd<sup>3+</sup>, which inhibits SOCE, restoration of extracellular Ca<sup>2+</sup> did not initiate SOCE and a decrease in the TIRFM signal was not observed (Fig. 1B). Store refilling in the absence of Gd<sup>3+</sup> was further verified by the fact that addition of thapsigargin, which depletes Ca<sup>2+</sup> stores by inhibiting SERCA pumps, caused a small Ca<sup>2+</sup> release and a subsequent increase in the TIRFM signal (Fig. 1A); these responses were not observed in the Gd<sup>3+</sup>-treated cells (Fig. 1B) because stores had not been refilled. It has been demonstrated that, when stores are full, EYFP-Stim1 exhibits constitutive comet-like movements when overexpressed in DT40 cells and that these movements cease as stores are depleted and EYFP-Stim1 rearranges into near-PM punctae (Baba et al., 2006). We observed similar constitutive movements of EYFP-Stim1 in HEK293 cells and further found that these movements were restored when the punctate EYFP-Stim1 localization was reversed by store refilling (supplementary material Movie 1).

It is apparent from the TIRFM imaging experiments of Fig. 1 that store refilling causes a significant reversal of EYFP-Stim1 localization; however, it is difficult to determine from TIRFM images whether EYFP-Stim1 returns to the same structures characteristic of the store-replete condition. We therefore performed similar experiments by confocal microscopy. As shown in Fig. 2A, EYFP-Stim1 is localized in tubular structures when Ca<sup>2+</sup> stores are full, and it rearranges into punctate structures when Ca<sup>2+</sup> stores are depleted by carbachol treatment. Store refilling upon restoration of extracellular Ca<sup>2+</sup> in the presence of atropine caused reversal of EYFP-Stim1 into tubular structures strikingly similar to those seen in the initial store-replete state. We have also observed, as shown by others (Luik et al., 2006; Xu et al., 2006; Varnai et al., 2007), that CFP-tagged Orai1 (CFP-Orai1) is localized evenly throughout the plasma membrane when Ca<sup>2+</sup> stores are replete but

rearranges into punctate structures that colocalize with those formed by EYFP-Stim1 when stores are emptied (Fig. 2B). These CFP-Orai1 punctae were also reversed by Ca<sup>2+</sup> store refilling, returning CFP-Orai1 to a localization similar to that seen in the initial store-replete state. As previously shown (Xu et al., 2006;

Varnai et al., 2007), CFP-Orai1 did not rearrange to an appreciable degree upon store depletion when Stim1 was not also overexpressed (supplementary material Fig. S1). Finally, Fig. 2 illustrates a general finding that, in some cells, Stim1 punctae appear small and discrete (Fig. 2A), whereas in others, the punctae take on more of a patchwork appearance (Fig. 2B). The reason for these differences is not clear, but we speculate that the larger structures arise with higher levels of EYFP-Stim1 expression. We do not generally observe these large patch-like aggregations of EYFP-Stim1 by TIRFM, which might indicate that significant areas of these structures lie beyond the Z-resolution of TIRFM.

#### ML-9 inhibits SOCE and $I_{crac}$

In an attempt to understand the underlying mechanism for Stim1 movement, we assessed the actions of a number of putative inhibitors of cytoskeletal function and molecular motors. One agent that gave particularly encouraging results was ML-9 [1-(5-chloronaphthalene-1-sulfonyl)homopiperazine, HCl], a drug known to inhibit myosin-light-chain kinase (MLCK) (Saitoh et al., 1986; Saitoh et al., 1987). Previous reports demonstrated inhibition of SOCE by ML-9, and this was taken as evidence for a role of myosin light chain kinase in this signaling pathway (Watanabe et al., 1996; Norwood et al., 2000; Tran et al., 2001). We analyzed SOCE in HEK293 cells using a standard  $Ca^{2+}$  add-back assay, whereby intracellular  $Ca^{2+}$  stores were depleted by treating cells with thapsigargin in the presence of nominal extracellular  $Ca^{2+}$ , followed by restoration of extracellular  $Ca^{2+}$  to 1.8 mM. When this assay was performed on cells that were treated with 100  $\mu$ M ML-9 for 5 minutes before store depletion with thapsigargin, SOCE was nearly completely absent compared with untreated control cells (Fig. 3A). DMSO, as a vehicle control for ML-9, had no effect. SOCE recovered to the same magnitude as untreated controls when ML-9 was removed 5 minutes following addition of extracellular  $Ca^{2+}$ , indicating that the inhibition of SOCE by ML-9 is rapidly reversible. The inhibition of SOCE by ML-9 was concentration dependent, with an  $IC_{50}$  of  $\sim 10$   $\mu$ M (Fig. 3B). Note that there was a small increase in intracellular  $Ca^{2+}$  at the time of ML-9 addition; such an effect was previously reported and was attributed to release of  $Ca^{2+}$  from intracellular stores by ML-9 (Norwood et al., 2000). It is likely that this  $Ca^{2+}$  increase that we observed is also due to a partial intracellular  $Ca^{2+}$  release by ML-9 as the amount of  $Ca^{2+}$  mobilized by thapsigargin was reduced in ML-9-treated cells. We also determined whether ML-9 is effective when added after SOCE has been initiated. To test this, we performed the  $Ca^{2+}$  add-back assay as described in the absence of ML-9 and then added ML-9 five minutes following restoration of extracellular  $Ca^{2+}$ . The addition of 100  $\mu$ M ML-9 caused the intracellular  $Ca^{2+}$  concentration to return rapidly to its basal level (Fig. 3C). To evaluate the extent of inhibition statistically, the intracellular  $Ca^{2+}$  concentration following the addition of ML-9 was divided by the  $Ca^{2+}$  concentration just before ML-9 addition; thus, the data are represented as the proportion of SOCE that remains following ML-9 as a function of the amount of SOCE present just before ML-9. This evaluation over a range of concentrations revealed a concentration-dependent inhibition by ML-9 ( $IC_{50} \approx 16$   $\mu$ M; Fig.

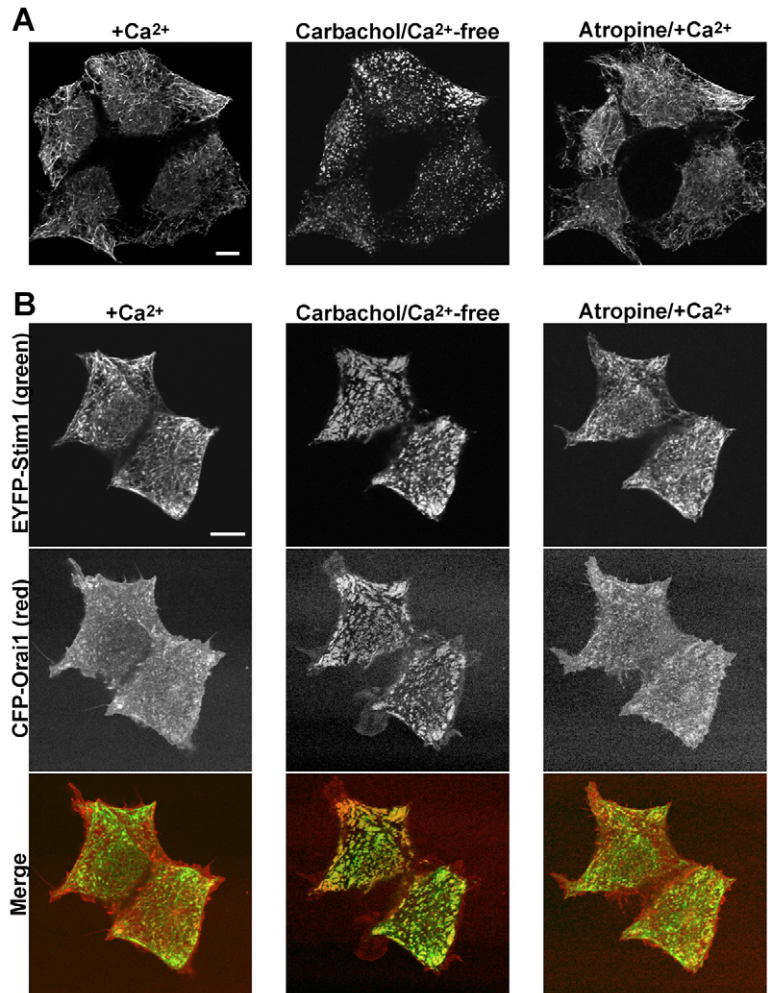


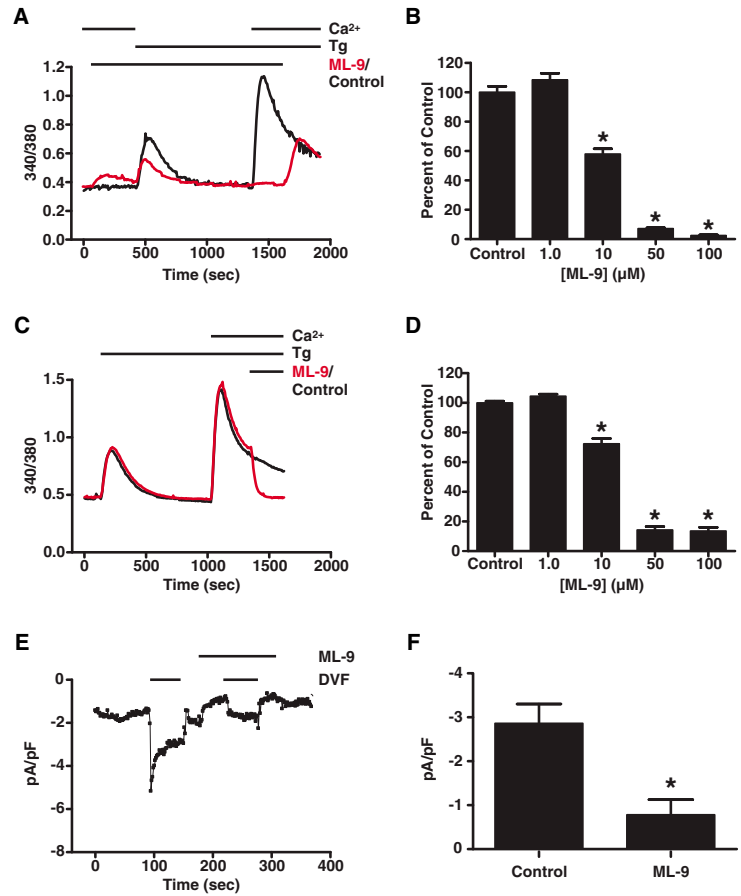
**Fig. 2.** Rearrangements of both Stim1 and Orai1 are reversed by  $Ca^{2+}$  store refilling. (A) Confocal images of HEK293 cells co-overexpressing EYFP-Stim1 and the m5 muscarinic receptor in the presence of 1.8 mM extracellular  $Ca^{2+}$  before store depletion (left panel), 10 minutes following treatment with 300  $\mu$ M carbachol in nominally  $Ca^{2+}$ -free extracellular solution (center panel), and 10 minutes following restoration of 1.8 mM extracellular  $Ca^{2+}$  in the presence of 50  $\mu$ M atropine (right panel). (B) The same protocol described in panel A was repeated with cells co-overexpressing EYFP-Stim1, CFP-Orai1 and the m5 muscarinic receptor. EYFP-Stim1 fluorescence is shown in the upper row, CFP-Orai1 is shown in the center row, and the bottom row shows merged images of EYFP-Stim1 (green) and CFP-Orai1 (red). Bars, 10  $\mu$ m.

3D) that was similar to that seen when ML-9 was added before activation of SOCE.

To confirm that the inhibition by ML-9 reflected a decrease in ion permeation of  $Ca^{2+}$ -release-activated  $Ca^{2+}$  (CRAC) channels, rather than effects on membrane potential or calcium buffering, we carried out electrophysiological measurements of the  $I_{crac}$  current in HEK293 cells in the absence and presence of ML-9. It is difficult to measure  $I_{crac}$  reliably in these cells when  $Ca^{2+}$  is used as the charge carrier because the currents are very small, on the order of  $-0.5$  pA/pF. However, a  $Na^{+}$  current can consistently be measured when the extracellular solution is switched to one that is free of all divalent cations. As shown in Fig. 3E, when 25  $\mu$ M  $Ins(1,4,5)P_3$  and 20 mM BAPTA were included in the patch pipette to deplete intracellular  $Ca^{2+}$  stores, a  $Na^{+}$  current of approximately  $-3$  to  $-4$  pA/pF was measured when the extracellular solution was switched



**Fig. 3.** ML-9 dose-dependently inhibits SOCE and  $I_{\text{crac}}$ . (A) Relative intracellular  $\text{Ca}^{2+}$  concentrations were monitored in wild-type HEK293 cells treated with 100  $\mu\text{M}$  ML-9 (red trace) or left untreated (black trace).  $\text{Ca}^{2+}$  stores were depleted with 2  $\mu\text{M}$  thapsigargin in nominally  $\text{Ca}^{2+}$ -free extracellular medium, and extracellular  $\text{Ca}^{2+}$  was restored to 1.8 mM 15 minutes later to reveal SOCE. ML-9 was removed at the end of the experiment to demonstrate the reversibility of ML-9 inhibition. Each trace represents the averaged response of all cells measured on a single coverslip. (B) The average peak SOCE responses above baseline from experiments performed as described in panel A were averaged for untreated control cells ( $n=150$ ; five coverslips) or cells treated with 1  $\mu\text{M}$  ( $n=78$ ; three coverslips), 10  $\mu\text{M}$  ( $n=76$ ; three coverslips), 50  $\mu\text{M}$  ( $n=84$ ; three coverslips) or 100  $\mu\text{M}$  ( $n=64$ ; three coverslips) ML-9. Data are reported as the percentage of untreated control  $\pm$  s.e.m.; \*, significant difference compared with control ( $P<0.001$ ) based on one-way ANOVA. (C) Experiments were performed as described in panel A, but ML-9 was added 5 minutes following restoration of extracellular  $\text{Ca}^{2+}$  (red trace). (D) For experiments performed as described in panel C, the baseline-subtracted 340/380 ratio 5 minutes following ML-9 addition was divided by that just before addition. Data are reported as the percentage of untreated control  $\pm$  s.e.m. for untreated controls ( $n=151$ ; five coverslips), and for 1  $\mu\text{M}$  ( $n=90$ ; four coverslips), 10  $\mu\text{M}$  ( $n=80$ , three coverslips), 50  $\mu\text{M}$  ( $n=61$ , three coverslips) and 100  $\mu\text{M}$  ( $n=74$ , three coverslips) ML-9; \*, significant difference compared with control ( $P<0.001$ ) based on one-way ANOVA. (E) Whole-cell patch clamp analysis was performed with a pipette solution containing 20 mM BAPTA and 25  $\mu\text{M}$  Ins(1,4,5) $\text{P}_3$  to deplete intracellular  $\text{Ca}^{2+}$  stores. The cell was initially perfused with an extracellular solution containing 10 mM  $\text{Ca}^{2+}$ . At the time indicated, perfusion was switched to a divalent-free (DVF) solution, which resulted in the development of a  $\text{Na}^+$  current. Perfusion was then returned to 10 mM  $\text{Ca}^{2+}$ , and 100  $\mu\text{M}$  ML-9 was added at the time indicated. Note the decrease in the  $\text{Ca}^{2+}$  current upon ML-9 addition. In the continued presence of ML-9, perfusion was again switched to DVF solution. At the end of the experiment, 10 mM extracellular  $\text{Ca}^{2+}$  was restored and ML-9 was removed to demonstrate reversal of inhibition of the  $\text{Ca}^{2+}$  current. (F) For experiments performed as described in panel E, the peak  $\text{Na}^+$  currents at the initial switch to DVF solution in the absence of ML-9 (control) and that at the second switch to DVF in the presence of 100  $\mu\text{M}$  ML-9 were averaged and are expressed as mean  $\pm$  s.e.m. ( $n=6$ ); \*, significant difference compared with control ( $P<0.005$ ) based on Student's  $t$  test.

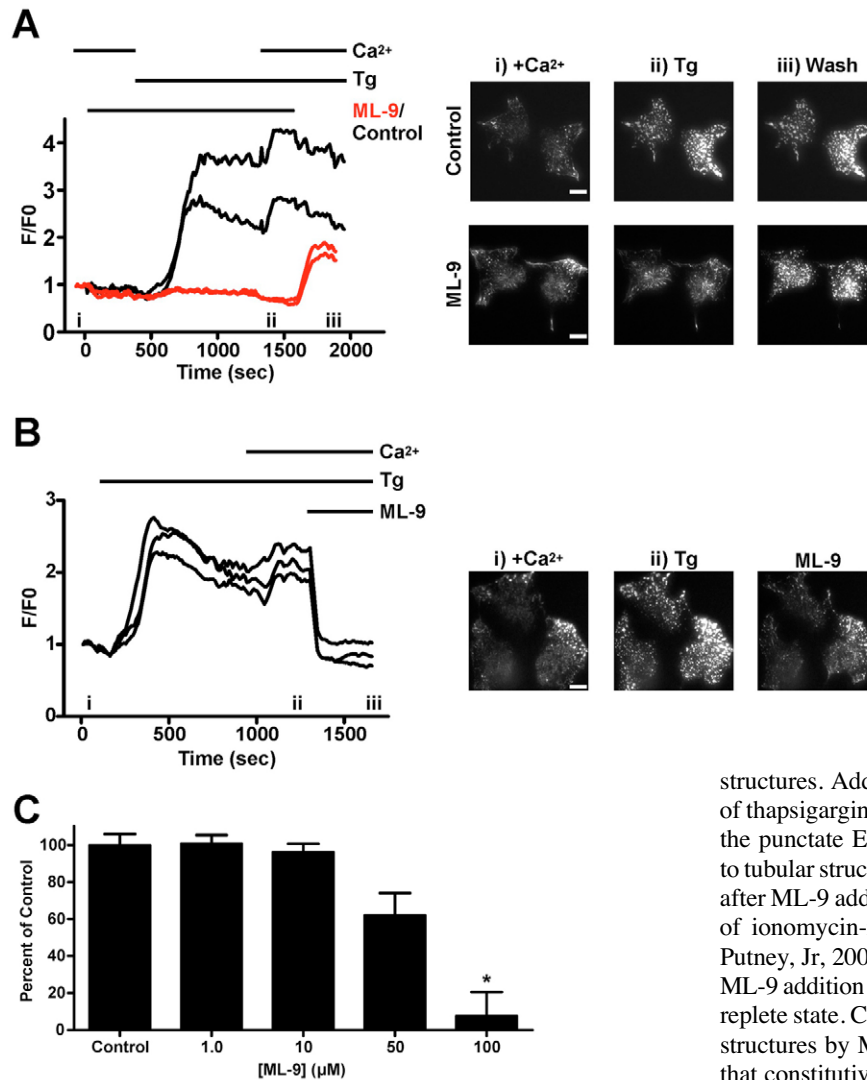


from 10 mM  $\text{Ca}^{2+}$  to being divalent free. The extracellular solution was then switched back to  $\text{Ca}^{2+}$ , and 100  $\mu\text{M}$  ML-9 was added. Notably, there was a decrease in the  $\text{Ca}^{2+}$  current when ML-9 was added, indicative of inhibition by ML-9. More importantly, the  $\text{Na}^+$  current was significantly inhibited when the extracellular solution was again switched to being divalent free in the continued presence of ML-9 (Fig. 3E,F). The residual current in the presence of ML-9 is not likely due to significant  $I_{\text{crac}}$ ; upon switching to divalent-free solutions in the absence of store depletion, we generally observe a linear increase in membrane current of the order of 0.6 pA/pF (DeHaven et al., 2007). Thus, ML-9 similarly inhibits SOCE and  $I_{\text{crac}}$  in HEK293 cells.

### ML-9 reverses rearrangement of Stim1

We hypothesized that ML-9 inhibits SOCE and  $I_{\text{crac}}$  by blocking the rearrangement of Stim1 that occurs when  $\text{Ca}^{2+}$  stores are depleted. To test this, we monitored EYFP-Stim1 rearrangement by TIRFM in experiments carried out in a manner similar to the SOCE experiments described in Fig. 3 – that is,  $\text{Ca}^{2+}$  stores were depleted with thapsigargin in a nominally  $\text{Ca}^{2+}$ -free extracellular solution, after which extracellular  $\text{Ca}^{2+}$  was restored to 1.8 mM. As seen in the control traces in Fig. 4A, the fluorescence intensity measured by TIRFM increased significantly following store depletion with thapsigargin. Unexpectedly, we consistently observed a further, albeit relatively small, increase in TIRFM fluorescence

when extracellular  $\text{Ca}^{2+}$  was restored; we do not currently know the cause of this  $\text{Ca}^{2+}$ -induced increase in near-PM EYFP-Stim1 localization, and this is a topic of further investigation in our laboratory. By contrast, cells treated with 100  $\mu\text{M}$  ML-9 for 5 minutes before store depletion exhibited little to no increase in TIRFM fluorescence intensity following store depletion or upon  $\text{Ca}^{2+}$  add-back, and EYFP-Stim1 puncta were not formed (Fig. 4A). However, the TIRFM fluorescence intensity rapidly increased when ML-9 was removed, indicating that, similar to the inhibition of SOCE, inhibition of EYFP-Stim1 rearrangement by ML-9 is reversible. Thus, the inhibitory properties of ML-9 in TIRFM experiments directly paralleled those observed in SOCE experiments. Likewise, as we found that ML-9 also blocked SOCE when added after its initiation, we examined the ability of ML-9 to reverse the near-PM localization of EYFP-Stim1 after rearrangement was induced by store depletion. In these TIRFM experiments,  $\text{Ca}^{2+}$  stores were depleted with thapsigargin in a nominally  $\text{Ca}^{2+}$ -free solution, resulting in a large TIRFM fluorescence intensity increase.  $\text{Ca}^{2+}$  was then restored to 1.8 mM (note again the small fluorescence intensity increase), and ML-9 (100  $\mu\text{M}$ ) was then added in the continued presence of 1.8 mM  $\text{Ca}^{2+}$  (Fig. 4B). Addition of ML-9 at this time-point caused the TIRFM fluorescence intensity to decrease rapidly to near-basal levels, indicative of reversal of near-PM EYFP-Stim1 localization. Similar TIRFM responses and reversal by ML-9 were seen when



stores were depleted with the receptor agonist carbachol (data not shown) or with 400 nM ionomycin (supplementary material Fig. S2). Thus, ML-9 effectively inhibited SOCE,  $I_{\text{crac}}$  and EYFP-Stim1 rearrangement whether it was added before or after store depletion. Because the order of ML-9 addition in relation to store depletion did not appear to significantly influence the concentration dependence of SOCE inhibition, we determined the concentration dependence of the inhibition of EYFP-Stim1 rearrangement from TIRFM experiments in which ML-9 was added after store depletion, as described in Fig. 4B. This allowed us to normalize the fluorescence intensity after ML-9 addition to that just before ML-9 addition for each cell individually (Fig. 4C). However, we were surprised to find that the concentration dependence for inhibition of EYFP-Stim1 rearrangement ( $\text{IC}_{50} \sim 51 \mu\text{M}$ ) was somewhat greater than that for SOCE. We will address this issue in a later section of this report.

To evaluate more closely the effects of ML-9 on EYFP-Stim1 localization, we imaged EYFP-Stim1-expressing HEK293 cells by confocal microscopy. As shown in Fig. 5, store depletion with thapsigargin in nominally  $\text{Ca}^{2+}$ -free extracellular solution caused rearrangement of EYFP-Stim1 from tubular into discrete punctate

**Fig. 4.** ML-9 inhibits EYFP-Stim1 rearrangement. (A) Time-lapse TIRFM was performed on EYFP-Stim1-overexpressing HEK293 cells treated with 100  $\mu\text{M}$  ML-9 or left untreated (control). The left panel shows TIRFM fluorescence intensity profiles for two control (black traces) and two ML-9-treated cells (red traces). Thapsigargin (Tg; 2  $\mu\text{M}$ ) was added in nominally  $\text{Ca}^{2+}$ -free extracellular solution at the time indicated to deplete  $\text{Ca}^{2+}$  stores, and ML-9 was removed at the end of the experiment to demonstrate reversal of the ML-9 inhibition. The right-hand panel shows representative TIRFM images taken at the times indicated (i-iii) in the intensity profile. (B) TIRFM imaging was performed on three cells as described in panel A, but ML-9 (100  $\mu\text{M}$ ) was added after store depletion with thapsigargin. (C) The average baseline-subtracted TIRFM fluorescence intensity 5 minutes following ML-9 addition was divided by that just before addition for experiments performed as described in panel B for untreated controls ( $n=6$ ; two coverslips), or cells treated with 1  $\mu\text{M}$  ( $n=11$ ; three coverslips), 10  $\mu\text{M}$  ( $n=11$ , three coverslips), 50  $\mu\text{M}$  ( $n=14$ , three coverslips) and 100  $\mu\text{M}$  ( $n=10$ , three coverslips) ML-9. Data are expressed as the percentage of untreated control  $\pm$  s.e.m.; \* significant difference compared with control ( $P < 0.001$ ) based on one-way ANOVA. Bars, 10  $\mu\text{m}$ .

structures. Addition of ML-9 (100  $\mu\text{M}$ ) in the continued presence of thapsigargin and nominal extracellular  $\text{Ca}^{2+}$  completely reversed the punctate EYFP-Stim1 localization, and EYFP-Stim1 returned to tubular structures. With this protocol,  $\text{Ca}^{2+}$  stores remained empty after ML-9 addition, as assessed by experiments examining the size of ionomycin-releasable  $\text{Ca}^{2+}$  pools (data not shown) (Bird and Putney, Jr, 2005). Notably, these tubular structures seen following ML-9 addition were nearly identical to those seen in the initial store-replete state. Consistent with the return of EYFP-Stim1 into tubular structures by ML-9, we also found in time-lapse TIRFM imaging that constitutive EYFP-Stim1 movements reinitiated when EYFP-Stim1 localization was reversed with 100  $\mu\text{M}$  ML-9 (supplementary material Movie 2). Thus, assessed by two independent measures, the reversal of EYFP-Stim1 localization by ML-9 appears to be complete.

#### Inhibition of $\text{Ca}^{2+}$ entry is due to inhibition of Stim1 rearrangement

It was apparent that the concentration dependence of inhibition of SOCE by ML-9 in wild-type (unconjugated-EYFP transfected) cells was more sensitive than that of the overexpressed EYFP-Stim1 rearrangement. One possibility for this discrepancy is that overexpression of EYFP-Stim1 in TIRFM experiments might shift the concentration dependence of inhibition. To test this more directly, we compared the concentration dependence of inhibition of SOCE by ML-9 in wild-type HEK293 cells overexpressing unconjugated EYFP with that in HEK293 cells overexpressing EYFP-Stim1. Data for this analysis were obtained by performing experiments as described in Fig. 3C in which ML-9 was added after the initiation of SOCE. The concentration-dependent responses for EYFP alone and EYFP-Stim1-expressing cells are shown in Fig. 6A. It is apparent that overexpression of EYFP-Stim1 caused a rightward shift in the concentration dependence, and the  $\text{IC}_{50}$  for inhibition of SOCE by ML-9 in EYFP-Stim1-expressing cells was 66  $\mu\text{M}$ , compared with 16  $\mu\text{M}$  in cells expressing unconjugated

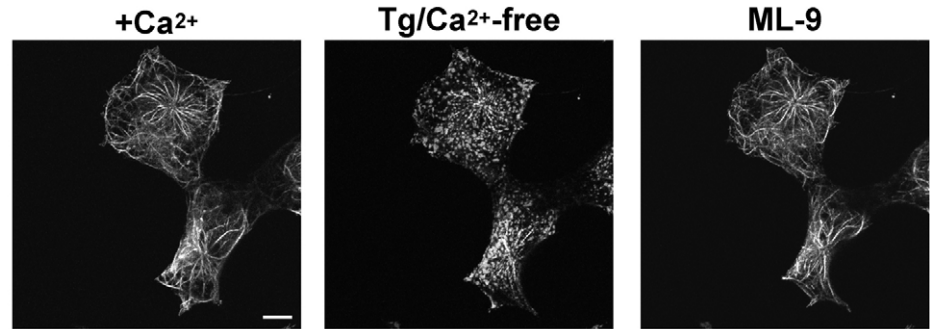


**Fig. 5.** Reversal of Stim1 localization by ML-9 is complete. Shown are confocal images of cells in the presence of 1.8 mM extracellular  $\text{Ca}^{2+}$  (left panel), 15 minutes following store depletion with thapsigargin (Tg; 2  $\mu\text{M}$ ) in nominally  $\text{Ca}^{2+}$ -free extracellular solution (center panel) and 5 minutes following addition of 100  $\mu\text{M}$  ML-9 in the continued presence of Tg and  $\text{Ca}^{2+}$ -free extracellular solution. Bars, 10  $\mu\text{m}$ .

EYFP. Furthermore, the  $\text{IC}_{50}$  for inhibition of SOCE in EYFP-Stim1-expressing cells was close to that for inhibition of EYFP-Stim1 rearrangement from TIRFM experiments. The fact that overexpression of EYFP-Stim1 has a rightward-shifting effect on the concentration dependence of SOCE inhibition by ML-9 provides strong evidence that the inhibition of SOCE is related to effects on Stim1 function.

We also analyzed the kinetics of inhibition of SOCE and EYFP-Stim1 rearrangement by simultaneously measuring the TIRFM fluorescence intensity and intracellular  $\text{Ca}^{2+}$  concentrations (Fig. 6B). In these experiments, thapsigargin was added to the cells in the presence of 1.8 mM extracellular  $\text{Ca}^{2+}$ ; thus, the  $\text{Ca}^{2+}$  response that is seen is representative of both an initial release from the ER as well as subsequent activation of SOCE. When 100  $\mu\text{M}$  ML-9 was added during the sustained SOCE phase, both the intracellular  $\text{Ca}^{2+}$  concentration and the TIRFM fluorescence intensity rapidly decreased to close to their original, basal levels (Fig. 6B). When both the  $\text{Ca}^{2+}$  and TIRFM responses to ML-9 were normalized to the same minimum and maximum scale, it was apparent that the decrease in TIRFM intensity preceded the decrease in  $\text{Ca}^{2+}$  concentration (Fig. 6C). This further supports the conclusion that the reversal of Stim1 localization by ML-9 is the cause of the inhibition of SOCE.

#### ML-9 inhibits a constitutively active mutant of Stim1

Mutations of  $\text{Ca}^{2+}$ -binding residues within the EF-hand domain of Stim1 render the mutated Stim1 constitutively active: the EF-hand-mutated Stim1 localizes in near-PM punctae even when intracellular  $\text{Ca}^{2+}$  stores are full, and constitutive SOCE is observed. As shown in Fig. 7A, cells that overexpress an EYFP-tagged human Stim1 in which the aspartic acids at positions 76 and 78 were mutated to asparagine residues (EYFP-D76N/D78N-Stim1) exhibit constitutive SOCE, as indicated by high intracellular  $\text{Ca}^{2+}$  levels that significantly decreased upon removal of extracellular  $\text{Ca}^{2+}$ , despite full intracellular  $\text{Ca}^{2+}$  stores. ML-9 inhibited this constitutive SOCE activity as the addition of 100  $\mu\text{M}$  ML-9 in the presence of 1.8 mM extracellular  $\text{Ca}^{2+}$  caused a rapid decrease in the intracellular  $\text{Ca}^{2+}$  concentration, and removal of extracellular  $\text{Ca}^{2+}$  in the continued presence of ML-9 resulted in only a small additional decrease. In TIRFM imaging, cells overexpressing EYFP-D76N/D78N-Stim1 exhibited intense near-PM punctae in the absence of store depletion, and, consistent with the  $\text{Ca}^{2+}$  data, the EYFP-D76N/D78N-Stim1 fluorescence intensity rapidly decreased upon addition of 100  $\mu\text{M}$  ML-9 (Fig. 7B). Remarkably, confocal imaging demonstrated that, when the constitutively punctate distribution of EYFP-D76N/D78N-Stim1 was reversed by ML-9, the construct adopted a tubular distribution that is indistinguishable from the configuration of wild-type EYFP-Stim1 in the presence

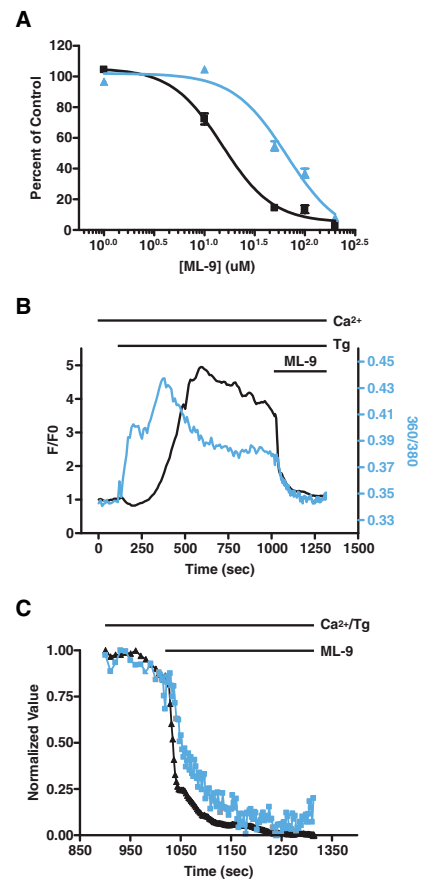


**Fig. 6.** Inhibition of SOCE and  $I_{\text{crac}}$  by ML-9 is due to inhibition of Stim1 rearrangement. (A) SOCE experiments were performed in which ML-9 was added following restoration of extracellular  $\text{Ca}^{2+}$  as described in Fig. 3C. As described in Fig. 3D, SOCE following ML-9 addition as a percentage of the untreated control was calculated and is plotted as a function of ML-9 concentration for HEK293 cells overexpressing untagged EYFP (black squares) and EYFP-Stim1 (blue triangles). (B) TIRFM fluorescence intensity (black trace) and relative intracellular  $\text{Ca}^{2+}$  concentration (360/380 ratio; blue trace) were measured simultaneously in the same cell.  $\text{Ca}^{2+}$  stores were depleted with thapsigargin (Tg; 2  $\mu\text{M}$ ) in the presence of 1.8 mM extracellular  $\text{Ca}^{2+}$ , and 100  $\mu\text{M}$  ML-9 was added 15 minutes later. (C) For the data shown in panel B, the TIRFM (black trace) and 360/380 (blue trace) values beginning just before ML-9 addition were normalized to the same minimum and maximum values.



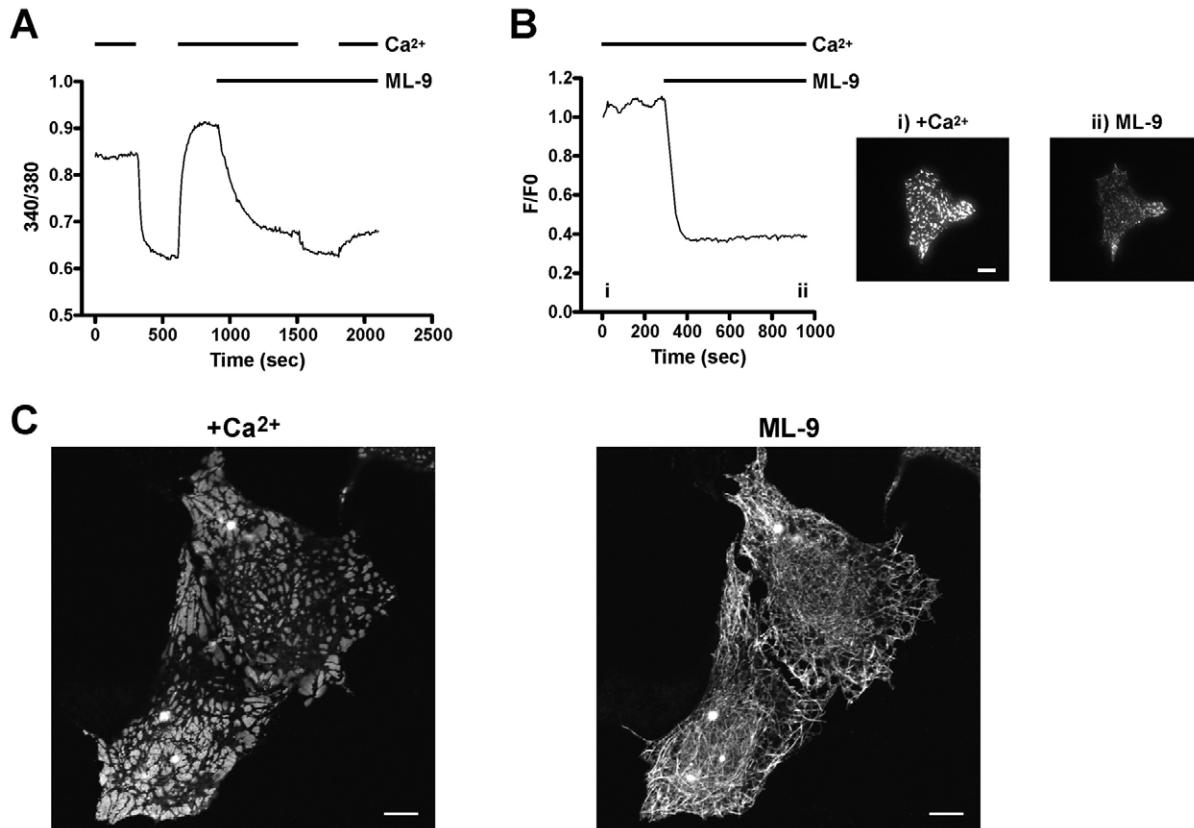


**Fig. 7.** ML-9 reverses constitutive EYFP-D76N/D78N-Stim1 localization and SOCE activity. (A) Intracellular Ca<sup>2+</sup> concentration was monitored in HEK293 cells overexpressing EYFP-D76N/D78N-Stim1 beginning in the presence of 1.8 mM extracellular Ca<sup>2+</sup>, followed at the time indicated by switch to a nominally Ca<sup>2+</sup>-free extracellular solution. Extracellular Ca<sup>2+</sup> was then restored, and 100  $\mu$ M ML-9 was added. In the continuous presence of ML-9, extracellular Ca<sup>2+</sup> was again removed and restored. The trace represents the average response of all the cells measured on a single coverslip; representative of three independent experiments. (B) Time-lapse TIRFM was performed on a cell overexpressing EYFP-D76N/D78N-Stim1; 100  $\mu$ M ML-9 was added at the time indicated in the fluorescence intensity profile (left panel). Right-hand panel: representative TIRFM images taken at the times indicated (i and ii) in the intensity profile. Representative of three independent experiments. (C) Confocal images of EYFP-D76N/D78N-Stim1-expressing cells in the absence (left panel) and presence (right panel) of 100  $\mu$ M ML-9 in the presence of 1.8 mM extracellular Ca<sup>2+</sup> throughout. Bars, 10  $\mu$ m.

of replete Ca<sup>2+</sup> stores (Fig. 7C). This striking relocalization of EYFP-D76N/D78N-Stim1 by ML-9 was further exemplified by the fact that EYFP-D76N/D78N-Stim1 began to exhibit constitutive movements when cells were treated with 100  $\mu$ M ML-9 in time-lapse TIRFM imaging (supplementary material Movie 3).

The effects of ML-9 on Stim1 are probably not due to inhibition of MLCK

We determined whether other methods of decreasing MLCK activity could mimic the effects on Stim1 function that we have observed with ML-9. As shown in Fig. 8A,B, transfection of HEK293 cells with two out of three siRNA constructs targeted to MLCK resulted in a significant reduction in expression of MLCK protein, whereas a control siRNA construct had no significant effect. However, the TIRFM responses to store depletion by thapsigargin were not inhibited in cells that were co-transfected with EYFP-Stim1 and the MLCK#3 siRNA construct (Fig. 8D), which reduced MLCK expression by approximately 80%, compared with the responses in cells transfected with the control siRNA (Fig. 8C). Expression of the other two MLCK siRNA constructs also had no inhibitory effect on the TIRFM response (data not shown). We also attempted to replicate pharmacologically the effects of ML-9. However, pretreatment of cells with 20  $\mu$ M

wortmannin, which inhibits MLCK activity (Nakanishi et al., 1992), had no effect on the TIRFM response of EYFP-Stim1 to store depletion (data not shown).

EYFP-Stim1 punctae form in predetermined locations

The ability to block reversibly the punctate localization of EYFP-Stim1 provided us with the opportunity to explore whether EYFP-Stim1 punctae form in similar locations in the same cell each time their formation is induced. If this is the case, then it would imply that cellular structures or molecules other than Stim1 itself determine the localization of Stim1 punctae formation. For this analysis, we used ML-9 to reverse EYFP-Stim1 localization as reversal with ML-9 was consistently more effective than that seen with any other strategy. As shown in the TIRFM fluorescence intensity profile in Fig. 9A and the representative images in Fig. 9B, store depletion with thapsigargin induced formation of EYFP-Stim1 punctae that was rapidly and completely reversed by 100  $\mu$ M ML-9. Upon washout of the ML-9, punctae rapidly reformed with a fluorescence intensity similar to that seen before ML-9 treatment. To compare the locations of EYFP-Stim1 punctae pre-reversal with ML-9 to those post-reversal (i.e. following washout of ML-9), a pre-reversal TIRFM image was pseudocolored red and merged with a post-reversal image that was pseudocolored green (Fig. 9C). These image

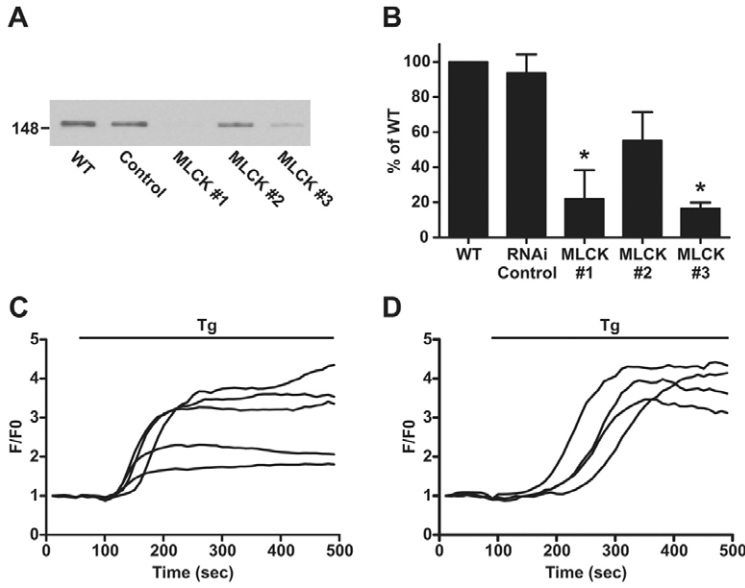


**Fig. 8.** Knockdown of MLCK protein expression by siRNA does not inhibit rearrangement of EYFP-Stim1. (A) HEK293 cells left untransfected (WT; lane 1), or transfected with control siRNA (lane 2) or one of three different MLCK siRNA constructs (lanes 3-5) were subjected to western blotting with an antibody against MLCK. (B) Three independent experiments were performed as described in panel A, and the average band intensities for each condition are expressed as a percentage of wild-type  $\pm$  s.e.m.; \*, significant difference compared with wild-type cells ( $P < 0.01$ ) based on one-way ANOVA. (C) Cells were transfected with control siRNA or (D) with MLCK #3, and TIRFM experiments were performed in which stores were depleted with 2  $\mu$ M thapsigargin in nominally  $Ca^{2+}$ -free extracellular solution. Each trace represents a single cell, and the responses of all the cells measured from a single coverslip are shown.

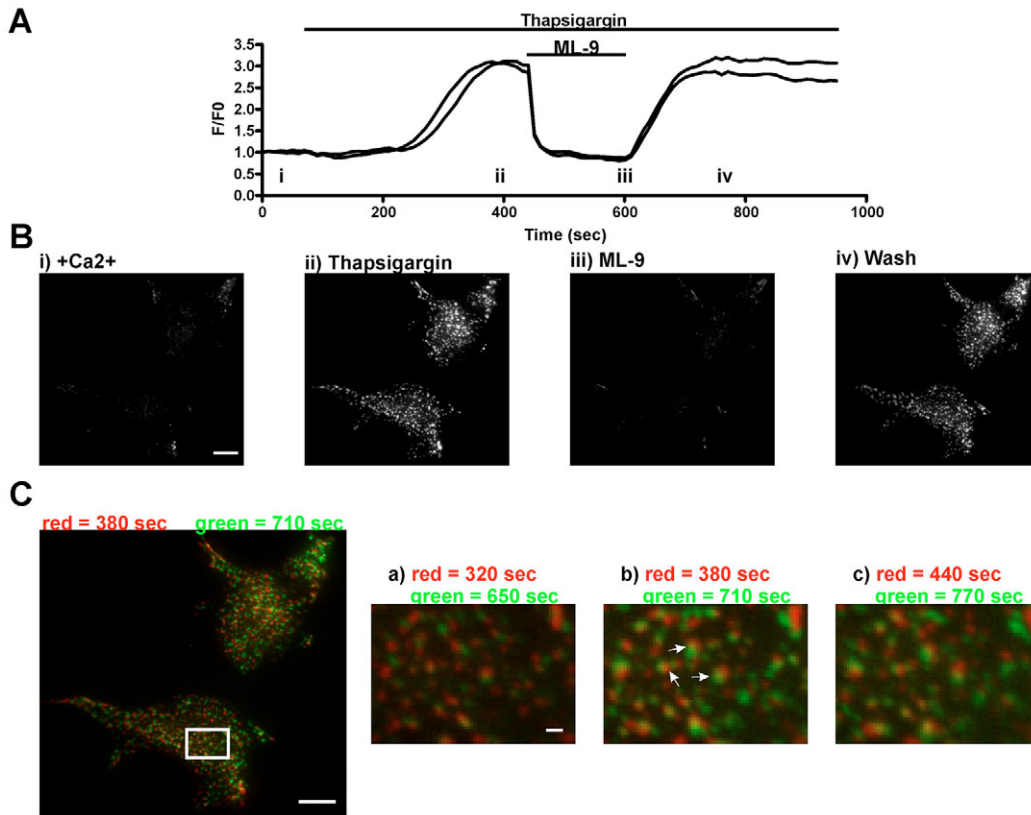


**Fig. 9.** Single EYFP-Stim1 punctae form in similar locations upon multiple rearrangement stimuli. (A) Two EYFP-Stim1-expressing HEK293 cells were imaged by time-lapse TIRFM, during which  $Ca^{2+}$  stores were depleted with 2  $\mu$ M thapsigargin in the presence of nominal extracellular  $Ca^{2+}$ , 100  $\mu$ M ML-9 was added to reverse punctae formation and ML-9 was removed to re-stimulate punctae formation. Shown is the fluorescence intensity profile, with each trace representing a single cell. (B) Representative TIRFM images taken at the times indicated (i-iv) in the intensity profile in panel A. The complete image series of this experiment is shown in supplementary material Movie 4. (C) The TIRFM image taken at 380 seconds (store-depleted with thapsigargin before ML-9 treatment) was pseudocolored red. This image was then merged with the image taken at 710 seconds (after ML-9 washout), which was pseudocolored green. Image 'b' on the right is a close-up of the region denoted by the white rectangle in the full-size image on the left. Image 'a' was generated from the merge of the images 60 seconds before the images used to generate the full-size image on the left, and image 'c' was generated from the merge of the images 60 seconds after the images used to generate the full-size image on the left. The arrows in image 'b' point to pairs of red and green punctae that remain consistent throughout the series of merged images. Scale bars: 10  $\mu$ m in B and C; 1  $\mu$ m in Ca-c.



manipulations revealed that many punctae were located in the same, or near to the same, position in the images taken pre- and post-reversal. Furthermore, evaluation of several merged images in sequence (Fig. 9C and supplementary material Movie 4) revealed that these closely apposed pre- and post-reversal punctae remained closely apposed over time, indicating that this correlation was not stochastic or specific to one pair of merged images. It should be noted that EYFP-Stim1 punctae do not remain static over time, but instead exhibit small lateral movements, as can be seen in the complete time-lapse movie of the experiment shown in Fig. 9 (supplementary material Movie 5). Thus, it is not expected that EYFP-Stim1 punctae should form in the exact same locations pre- and post-reversal, and is it reasonable to expect that there might be some regions of the cell where there is little correlation between the pre- and post-reversal punctae. More importantly, in all three experiments performed in this manner, we were able to find regions of the cells where clear spatial coincidence between pre- and post-reversal punctae was apparent.

## Discussion

### Physiological reversal of Stim1 and Orai1 localization by store refilling

Since the discovery of the role of Stim1 in SOCE, the majority of studies have focused on the mechanisms by which Stim1 rearranges into near-PM punctae and activates  $\text{Ca}^{2+}$  entry. It is equally important, however, that we also understand the mechanisms by which SOCE is terminated. Unregulated  $\text{Ca}^{2+}$  entry could lead to overload of cytoplasmic and/or ER  $\text{Ca}^{2+}$ , both of which can be detrimental to cellular physiology. Furthermore, discrete  $\text{Ca}^{2+}$  signals, such as  $\text{Ca}^{2+}$  oscillations, might depend on tightly controlled SOCE events (Bird and Putney, Jr, 2005; Wedel et al., 2007). The reversibility of Stim1 rearrangement has previously been established (Liou et al., 2005; Varnai et al., 2007), and we have now clearly demonstrated that this reversibility absolutely requires  $\text{Ca}^{2+}$  store refilling through store-operated calcium (SOC) channels. It is also apparent that, upon reversal, Stim1 localizes into tubular structures that are analogous to those seen before store depletion. Consistent with this, we also observed constitutive, comet-like movements of reversed EYFP-Stim1 that are typical of those exhibited by EYFP-Stim1 before store depletion (Baba et al., 2006). Thus, by all measures, EYFP-Stim1 reverses to its basal state upon store refilling, allowing it to respond to subsequent store-depletion events, as evidenced by the ability of store depletion with thapsigargin to trigger rearrangement of EYFP-Stim1 into punctae after store refilling-induced reversal. We also report for the first time that the rearrangement of Orai1 into punctate structures as a result of  $\text{Ca}^{2+}$  store depletion is similarly reversed by store refilling. Thus, the two basic components of the SOCE machinery are completely reversed by store refilling through the SOC channels. The fact that overexpressed Orai1 does not rearrange to a significant degree in response to store depletion in cells that do not also overexpress Stim1 implies that rearrangement of Stim1 directs the rearrangement of Orai1, although this has yet to be proven. Our data are consistent with this in that reversal of Stim1 localization occurs concomitantly with reversal of Orai1 localization.

### Reversal of Stim1 localization by ML-9

We have, for the first time, demonstrated inhibition of store depletion-induced rearrangement of EYFP-Stim1 into near-PM punctae by a method that does not involve replenishment of  $\text{Ca}^{2+}$  stores, namely by use of the pharmacological agent ML-9. We have

also established that the ability of ML-9 to inhibit SOCE and  $I_{\text{crac}}$  is attributable to its inhibition of Stim1 localization into punctae. This finding is highly significant, given the lack of SOCE inhibitors for which the molecular basis of inhibition within the SOCE pathway has been established.

In SOCE experiments, the  $\text{IC}_{50}$  for inhibition by ML-9 is similar whether the compound is added before or after activation of SOCE. Thus, it appears that ML-9 is equally as effective at reversing SOCE as it is at preventing its activation. We obtained similar results in TIRFM experiments in that ML-9 effectively prevented store depletion-induced rearrangement of EYFP-Stim1 into near-PM punctae as well as reversed this PM localization after it was established. The  $\text{IC}_{50}$  for reversal of the TIRFM response in EYFP-Stim1-expressing cells was significantly greater than that for reversal of SOCE in wild-type cells, but was similar to that for reversal of SOCE in cells that overexpressed EYFP-Stim1. Unfortunately, a lack of antibodies against Stim1 suitable for immunofluorescence in wild-type cells has prevented us from evaluating the effect of ML-9 on rearrangement of endogenous Stim1. However, it appears from our data that, in the case of overexpressed EYFP-Stim1, the amount of EYFP-Stim1 that is localized in punctae as a function of ML-9 inhibition directly correlates with the extent of SOCE, based on the similarities between the inhibition curves. This is, to our knowledge, the first demonstration of a quantitative correspondence between the amount of Stim1 localized in near-PM punctae and the magnitude of SOCE. It also provides strong evidence indicating that the inhibition of SOCE by ML-9 is a result of inhibition of Stim1 localization. Why overexpression of EYFP-Stim1 reduces the efficacy of inhibition by ML-9 of EYFP-Stim1 rearrangement is unclear. Further evidence supporting the conclusion that ML-9 inhibits SOCE by reversing Stim1 localization comes from simultaneous TIRFM and intracellular  $\text{Ca}^{2+}$  measurements, in which the reversal of EYFP-Stim1 localization precedes that of SOCE. This is, in effect, a functional corollary of the recent finding that rearrangement of EYFP-Stim1 to the PM precedes the initiation of  $I_{\text{crac}}$  (Wu et al., 2006).

Closer examination of the reversal of EYFP-Stim1 localization by confocal microscopy revealed that EYFP-Stim1 reformed tubular structures upon ML-9 treatment that were nearly identical to those observed before store depletion. Furthermore, constitutive movements of EYFP-Stim1 were also observed following reversal by ML-9. Thus, similar to the reversal achieved by means of store refilling, reversal by ML-9 re-established the basal, store-replete localization and behavior of EYFP-Stim1. This is quite remarkable given that, in the case of ML-9 treatment,  $\text{Ca}^{2+}$  stores remained empty and yet EYFP-Stim1 still localized to the same structures typical of the store-replete state. Thus, ER  $\text{Ca}^{2+}$  is not required per se for EYFP-Stim1 to localize in tubular structures. Consistent with this is the fact that EYFP-D76N/D78N-Stim1, which is constitutively arranged in near-PM punctae regardless of  $\text{Ca}^{2+}$  store content, becomes localized to tubular structures and exhibits constitutive movements in response to ML-9 treatment. In this case, EYFP-D76N/D78N-Stim1 is able to localize to tubular structures in the same manner as wild-type Stim1, despite the fact that it harbors a mutation that renders it insensitive to ER  $\text{Ca}^{2+}$  concentrations. This finding also demonstrates that ML-9 does not simply substitute for  $\text{Ca}^{2+}$  by binding to the N-terminal  $\text{Ca}^{2+}$  binding site.

The mechanism by which ML-9 inhibits EYFP-Stim1 rearrangement is unclear at this point. Previous studies that have demonstrated inhibition of SOCE by ML-9 have generally attributed this effect to inhibition of MLCK, the characterized target of ML-

9 (Watanabe et al., 1996; Takahashi et al., 1997; Norwood et al., 2000). However, this conclusion has only been corroborated with molecular data in one study, in which an antisense oligonucleotide targeted to the gene encoding MLCK inhibited SOCE in human monocytes/macrophages (Tran et al., 2001). In our hands, significant knockdown of MLCK protein expression by siRNA did not have any measurable effect on store-depletion-induced rearrangement of EYFP-Stim1. Furthermore, wortmannin, which is also known to inhibit MLCK (Nakanishi et al., 1992), had no effect on EYFP-Stim1 rearrangement. A related point is that  $I_{crac}$  develops optimally when intracellular  $Ca^{2+}$  is buffered to extremely low levels, in which case MLCK, a  $Ca^{2+}$ /calmodulin-activated enzyme (Somlyo and Somlyo, 2003), would be essentially inactive. It therefore appears unlikely that MLCK plays a significant role in the activation mechanism for SOC channels, and thus inhibition of MLCK by ML-9 is unlikely to underlie the inhibition of Stim1 rearrangement and SOCE. Notably, ML-9 did not significantly affect the structure of the ER when monitored by confocal microscopy or TIRFM (data not shown). Thus, it also seems unlikely that the effects of ML-9 on Stim1 function are due to effects on ER structure, although changes at the ultrastructural level cannot be ruled out. Alternatively, it is possible that ML-9 might directly influence the conformation of Stim1, or might alter Stim1 phosphorylation, given that Stim1 has been demonstrated to be a phosphoprotein (Manji et al., 2000). The mechanism by which ML-9 affects Stim1 function might reveal important information on the activation mechanism of this important signaling protein and will be a topic of further research.

#### EYFP-Stim1 forms similarly localized punctae upon multiple stimulations

We have taken advantage of the reversibility of EYFP-Stim1 by store refilling and ML-9 treatment to demonstrate that EYFP-Stim1 forms punctae in similar locations upon multiple stimulations. This indicates that the locations of Stim1 punctae formation are governed by cellular components other than Stim1 itself and are not random in nature. In these experiments, the reversal of EYFP-Stim1 punctae was complete in as much as punctae were no longer visible by TIRFM; therefore, it is unlikely that small amounts of EYFP-Stim1 remained at the PM and directed the reversed EYFP-Stim1 back to the same sites. Furthermore, our demonstration that Orai1 also reverses upon store refilling suggests that Orai1 does not direct EYFP-Stim1 into the same punctae upon subsequent stimulations. Thus, molecules other than Stim1 and Orai1 might be involved in localizing Stim1 and Orai1 in punctae, as has recently been suggested (Varnai et al., 2007). It has also been demonstrated that, when stores are depleted, Stim1 localizes in punctae at sites of close apposition between the ER and the PM (Wu et al., 2006; Varnai et al., 2007); therefore, it is likely that these areas of ER-PM contact ultimately define the sites of Stim1 and Orai1 interaction.

In conclusion, Stim1 and Orai1 rearrangements induced by  $Ca^{2+}$  store depletion are completely reversed by store refilling, a finding that provides a molecular basis for the self-regulating nature of the SOCE process. Stim1 rearrangement can also be reversed experimentally with ML-9, independently of  $Ca^{2+}$  store content. Elucidation of the mechanism by which ML-9 affects Stim1 function could help reveal the mechanisms by which Stim1 localization is regulated. Finally, the reversibility of Stim1 rearrangement has allowed us to determine that the sites of formation of Stim1 punctae are governed by additional, as-yet-unidentified molecular determinants.

## Materials and Methods

### Cell culture and transfections

Human embryonic kidney HEK293 cells were obtained from the ATCC and cultured in Dulbecco's modified Eagle's medium supplemented with 10% fetal bovine serum and 2 mM glutamine (DMEM) in a 37°C, 5%  $CO_2$  humidified incubator. Transfections of cDNA were performed using the Lipofectamine 2000 reagent (Invitrogen). EYFP-Stim1 was obtained from Tobias Meyer (Stanford University, CA); CFP-Orai1 was made in our laboratory by fusion of CFP to Orai1, purchased from Invitrogen, as described previously (DeHaven et al., 2007); and the m5 muscarinic receptor plasmid was obtained from Lutz Birnbaumer, NIEHS, Research Triangle Park, NC. EYFP-D76N/D78N-Stim1 was generated in our laboratory by site-directed mutagenesis of the construct obtained from Tobias Meyer, as previously described (Mercer et al., 2006). For transfections, 0.5  $\mu$ g of the EYFP-Stim1, EYFP-D76N/D78N-Stim1 and CFP-Orai1 plasmids were used, and 1.0  $\mu$ g of the m5 muscarinic receptor plasmid was used. In indicated experiments, cells were transfected with the plasmid encoding the m5 muscarinic receptor to enhance the responsiveness of cells to the muscarinic receptor agonist carbachol.

### Intracellular $Ca^{2+}$ measurements

Single-cell  $Ca^{2+}$  concentrations were measured in live cells plated on glass coverslips and mounted in Teflon chambers. Before experiments, cells were incubated in 1  $\mu$ M Fura-5F/AM (Invitrogen) for 25 minutes in DMEM at 37°C. Cells were then bathed in HEPES-buffered saline solution (HBSS: 120 mM NaCl, 5.4 mM KCl, 1.8 mM  $CaCl_2$ , 0.8 mM  $MgCl_2$ , 11 mM glucose and 20 mM HEPES, pH 7.4) throughout the course of the experiments. Fura-5F fluorescence was measured when cells were excited consecutively at 340 nm and 380 nm using a microscope-based digital fluorescence imaging system (InCyT Im2; Intracellular Imaging), and relative  $Ca^{2+}$  concentrations are reported as the ratio of fluorescence emission at the two excitation wavelengths. At the end of each experiment, Fura-5F/AM fluorescence was quenched by treating cells with 10  $\mu$ M ionomycin and 20 mM  $MnCl_2$  to obtain background fluorescence values; these background values were subtracted from each experimental measurement. Cells transfected with unconjugated EYFP or EYFP-Stim1 were identified based on their fluorescence emission at 530 nm when excited at 477 nm.

### Live-cell confocal and TIRFM imaging

Confocal and TIRFM imaging were performed on cells bathed in HBSS. All confocal images were obtained with a pinhole setting of 1 Airy Unit using a Zeiss LSM 510 laser scanning system and a 63 $\times$  oil-immersion (NA 1.4) lens. For EYFP-Stim1, 488 nm or 514 nm illumination was provided by an Argon laser and emission was selected with a 530-600 nm bandpass filter. The excitation for CFP-Orai1 was 458 nm from an Argon laser and emission was selected with a 470-510 nm bandpass filter. When cells expressing multiple probes were imaged, lack of bleed-through between channels was verified by imaging cells that expressed each of the probes individually. TIRFM was performed using an Olympus IX2 illumination system mounted on an Olympus IX71 inverted microscope. Excitation light was provided by a 488 nm argon ion laser (Melles Griot) directed through a fiber optic cable. The angle of illumination incident on the interface between the glass coverslip and the aqueous medium was controlled by adjusting the lateral position of the laser beam before passing through a 60 $\times$  oil-immersion objective (NA 1.45). The emitted fluorescence passed through a D525/50 nm filter (Chroma) and was captured by a Photometrics Cascade 512F cooled CCD (Roper Scientific). Acquisition and image analysis were performed using MetaFluor software (Molecular Devices). For fluorescence intensity profiles, data are represented as the fluorescence intensity at each time-point divided by the fluorescence intensity at the start of the experiment (F/F<sub>0</sub>). Fluorescence intensities were collected from regions of interest encompassing the visible footprints of single cells and were background subtracted. Time-lapse movies of TIRFM images were generated using ImageJ software. For simultaneous TIRFM and intracellular  $Ca^{2+}$  measurements, cells were first loaded with Fura-5F as described above, and each TIRFM image acquisition was immediately followed by a pair of acquisitions with excitation at 360 nm and 380 nm and emission at 525 nm. The 360 nm emission was chosen because the TIRFM objective did not transmit 340 nm light effectively. Excitation for Fura-5F measurements was provided by a 75W Xenon Arc lamp (Zeiss) and excitation and emission filters were controlled by a Lambda 10-2 filter wheel (Sutter Instruments). Intensity measurements at 360 nm and 380 nm were independently background subtracted, and data are presented as 360/380 ratios.

### Patch-clamp electrophysiology

Whole-cell currents were measured as described previously (DeHaven et al., 2007). The standard extracellular HBSS contained: 145 mM NaCl, 3 mM KCl, 10 mM CsCl, 1.2 mM  $MgCl_2$ , 10 mM  $CaCl_2$ , 10 mM glucose and 10 mM HEPES (adjusted to pH 7.4 with NaOH). The standard divalent-free (DVF) solution was prepared by removing the  $CaCl_2$  and  $MgCl_2$  from the HEPES solution and adding 0.1 mM EGTA. The intracellular pipette solution contained: 145 mM Cs-methanesulfonate, 20 mM BAPTA, 10 mM HEPES and 8 mM  $MgCl_2$  (adjusted to pH 7.2 with CsOH) together with the addition of 25  $\mu$ M Ins(1,4,5) $P_3$  (hexasodium salt). Currents were acquired with pCLAMP-10 (Axon Instruments) and analyzed with Clampfit (Axon Instruments).

## siRNA knockdown of MLCK expression

siRNA constructs targeted against expression of human MLCK were obtained from Invitrogen (Stealth RNAi); these constructs are predicted to suppress all MLCK isoforms with equal efficacy. The MLCK siRNA constructs had the following sequences: #1, AUAGAGGACAGUCUCCAUGGCUC; #2, CAAUCUUGCA-GUCAAAUCUAGCAGC; #3, UAGUCUAUCUGGAAGUGGCGGGACU. The control siRNA construct was the Stealth RNAi Negative Control Medium GC (Invitrogen). siRNA was transfected into cells using Metafectine reagent (Biontex) at a final concentration of 100 nM; cells were co-transfected with EYFP cDNA to identify transfected cells. Cells were assayed 48-72 hours following siRNA transfection.

## Western blotting

Cells were lysed in RIPA buffer (50 mM Tris HCl, 150 mM NaCl, 1 mM EDTA, 1% v/v Nonidet P-40, 0.25% w/v sodium deoxycholate, 1 mM phenylmethylsulfonyl fluoride, pH 7.5) containing one Complete Mini Protease Inhibitor Tablet (Roche Applied Sciences) per 10 ml, and total protein content in the lysates was determined using the DC Protein Assay Kit (BioRad). Lysates were normalized based on protein content and were electrophoresed in 6% polyacrylamide gels. Proteins were then transferred electrophoretically to PVDF membranes. Membranes were blocked for 1 hour at room temperature in TBS-T (24.7 mM Tris base, 137 mM NaCl, 2.7 mM KCl, 0.1% Tween-20, pH 7.4) containing 2% bovine serum albumin (BSA), incubated in primary antibody (mouse monoclonal anti-MLCK clone K36, Sigma) in TBS-T with BSA overnight at 4°C, and in secondary antibody (horseradish-peroxidase-linked anti-mouse IgG, Amersham) in TBS-T with BSA for 1 hour at room temperature. Membranes were washed for 10 minutes in TBS-T three times following each antibody incubation. Membranes were developed using ECL reagent (Amersham) and were exposed to film (Hyperfilm, Amersham). Band intensities were analyzed using Photoshop software.

## Reagents

ML-9 and wortmannin were obtained from Calbiochem; both compounds were dissolved in DMSO. Thapsigargin was obtained from Alexis Biochemicals. All other reagents were from Sigma unless stated otherwise.

Steven Shears and David Miller read the manuscript and provided useful comments. This research was supported by the Intramural Research Program of the NIH, National Institute of Environmental Health Sciences.

## References

- Baba, Y., Hayashi, K., Fujii, Y., Mizushima, A., Watarai, H., Wakamori, M., Numaga, T., Mori, Y., Iino, M., Hikida, M. et al. (2006). Coupling of STIM1 to store-operated Ca<sup>2+</sup> entry through its constitutive and inducible movement in the endoplasmic reticulum. *Proc. Natl. Acad. Sci. USA* **103**, 16704-16709.
- Bird, G. S. and Putney, J. W., Jr (2005). Capacitative calcium entry supports calcium oscillations in human embryonic kidney cells. *J. Physiol.* **562**, 697-706.
- DeHaven, W. I., Smyth, J. T., Boyles, R. R. and Putney, J. W., Jr (2007). Calcium inhibition and calcium potentiation of Orai1, Orai2, and Orai3 calcium release-activated calcium channels. *J. Biol. Chem.* **282**, 17548-17556.
- Dziadek, M. A. and Johnstone, L. S. (2007). Biochemical properties and cellular localisation of STIM proteins. *Cell Calcium* **42**, 123-132.
- Feske, S., Gwack, Y., Prakriya, M., Srikanth, S., Puppel, S. H., Tanasa, B., Hogan, P. G., Lewis, R. S., Daly, M. and Rao, A. (2006). A mutation in Orai1 causes immune deficiency by abrogating CRAC channel function. *Nature* **441**, 179-185.
- Liou, J., Kim, M. L., Heo, W. D., Jones, J. T., Myers, J. W., Ferrell, J. E., Jr and Meyer, T. (2005). STIM is a Ca<sup>2+</sup> sensor essential for Ca<sup>2+</sup>-store-depletion-triggered Ca<sup>2+</sup> influx. *Curr. Biol.* **15**, 1235-1241.
- Luik, R. M., Wu, M. M., Buchanan, J. and Lewis, R. S. (2006). The elementary unit of store-operated Ca<sup>2+</sup> entry: local activation of CRAC channels by STIM1 at ER-plasma membrane junctions. *J. Cell Biol.* **174**, 815-825.
- Manji, S. S., Parker, N. J., Williams, R. T., Van Stekelenburg, L., Pearson, R. B., Dziadek, M. and Smith, P. J. (2000). STIM1: a novel phosphoprotein located at the cell surface. *Biochim. Biophys. Acta* **1481**, 147-155.
- Mercer, J. C., DeHaven, W. I., Smyth, J. T., Wedel, B., Boyles, R. R., Bird, G. S. and Putney, J. W., Jr (2006). Large store-operated calcium-selected currents due to co-expression of orai1 or orai2 with the intracellular calcium sensor, stim1. *J. Biol. Chem.* **281**, 24979-24990.
- Nakanishi, S., Kakita, S., Takahashi, I., Kawahara, K., Tsukuda, E., Sano, T., Yamada, K., Yoshida, M., Kase, H. and Matsuda, Y. (1992). Wortmannin, a microbial product inhibitor of myosin light chain kinase. *J. Biol. Chem.* **267**, 2157-2163.
- Norwood, N., Moore, T. M., Dean, D. A., Bhattacharjee, R., Li, M. and Stevens, T. (2000). Store-operated calcium entry and increased endothelial cell permeability. *Am. J. Physiol. Lung Cell Mol. Physiol.* **279**, L815-L824.
- Parekh, A. B. and Putney, J. W., Jr (2005). Store-operated calcium channels. *Physiol. Rev.* **85**, 757-810.
- Saitoh, M., Naka, M. and Hidaka, H. (1986). The modulatory role of myosin light chain phosphorylation in human platelet activation. *Biochem. Biophys. Res. Commun.* **140**, 280-287.
- Saitoh, M., Ishikawa, T., Matsushima, S., Naka, M. and Hidaka, H. (1987). Selective inhibition of catalytic activity of smooth muscle myosin light chain kinase. *J. Biol. Chem.* **262**, 7796-7801.
- Smyth, J. T., DeHaven, W. I., Jones, B. F., Mercer, J. C., Trebak, M., Vazquez, G. and Putney, J. W., Jr (2006). Emerging perspectives in store-operated Ca<sup>2+</sup> entry: roles of Orai, Stim and TRP. *Biochim. Biophys. Acta* **1763**, 1147-1160.
- Smyth, J. T., DeHaven, W. I., Bird, G. S. and Putney, J. W., Jr (2007). Role of the microtubule cytoskeleton in the function of the store-operated Ca<sup>2+</sup> channel activator, Stim1. *J. Cell Sci.* **120**, 3762-3771.
- Soboloff, J., Spassova, M. A., Tang, X. D., Hewavitharana, T., Xu, W. and Gill, D. L. (2006). Orai1 and STIM reconstitute store-operated calcium channel function. *J. Biol. Chem.* **281**, 20661-20665.
- Somlyo, A. P. and Somlyo, A. V. (2003). Ca<sup>2+</sup> sensitivity of smooth muscle and nonmuscle myosin II: modulated by G proteins, kinases, and myosin phosphatase. *Physiol. Rev.* **83**, 1325-1358.
- Stathopoulos, P. B., Li, G. Y., Plevin, M. J., Ames, J. B. and Ikura, M. (2006). Stored Ca<sup>2+</sup> depletion-induced oligomerization of Stromal Interaction Molecule 1 (STIM1) via the EF-SAM region: an initiation mechanism for capacitive Ca<sup>2+</sup> entry. *J. Biol. Chem.* **281**, 35855-35862.
- Takahashi, R., Watanabe, H., Zhang, X. X., Kakizawa, H., Hayashi, H. and Ohno, R. (1997). Roles of inhibitors of myosin light chain kinase and tyrosine kinase on cation influx in agonist-stimulated endothelial cells. *Biochem. Biophys. Res. Commun.* **235**, 657-662.
- Tran, Q. K., Watanabe, H., Le, H. Y., Pan, L., Seto, M., Takeuchi, K. and Ohashi, K. (2001). Myosin light chain kinase regulates capacitative Ca<sup>2+</sup> entry in human monocytes/macrophages. *Arterioscler. Thromb. Vasc. Biol.* **21**, 509-515.
- Varnai, P., Toth, B., Toth, D. J., Hunyady, L. and Balla, T. (2007). Visualization and manipulation of plasma membrane-endoplasmic reticulum contact sites indicates the presence of additional molecular components within the STIM1-Orai1 complex. *J. Biol. Chem.* **282**, 29678-29690.
- Vig, M., Peinelt, C., Beck, A., Koormo, D. L., Rabah, D., Koblan-Huberson, M., Kraft, S., Turner, H., Fleig, A., Penner, R. et al. (2006). CRACM1 is a plasma membrane protein essential for store-operated Ca<sup>2+</sup> entry. *Science* **312**, 1220-1223.
- Watanabe, H., Takahashi, R., Zhang, X. X., Kakizawa, H., Hayashi, H. and Ohno, R. (1996). Inhibition of agonist-induced Ca<sup>2+</sup> entry in endothelial cells by myosin light-chain kinase inhibitor. *Biochem. Biophys. Res. Commun.* **225**, 777-784.
- Wedel, B., Boyles, R. R., Putney, J. W. and Bird, G. S. (2007). Role of the store-operated calcium entry proteins, Stim1 and Orai1, in muscarinic-cholinergic receptor stimulated calcium oscillations in human embryonic kidney cells. *J. Physiol.* **579**, 679-689.
- Wu, M. M., Buchanan, J., Luik, R. M. and Lewis, R. S. (2006). Ca<sup>2+</sup> store depletion causes STIM1 to accumulate in ER regions closely associated with the plasma membrane. *J. Cell Biol.* **174**, 803-813.
- Xu, P., Lu, J., Li, Z., Yu, X., Chen, L. and Xu, T. (2006). Aggregation of STIM1 underneath the plasma membrane induces clustering of Orai1. *Biochem. Biophys. Res. Commun.* **350**, 969-976.
- Zhang, S. L., Yu, Y., Roos, J., Kozak, J. A., Deerinck, T. J., Ellisman, M. H., Stauderman, K. A. and Cahalan, M. D. (2005). STIM1 is a Ca<sup>2+</sup> sensor that activates CRAC channels and migrates from the Ca<sup>2+</sup> store to the plasma membrane. *Nature* **437**, 902-905.
- Zhang, S. L., Yeromin, A. V., Zhang, X. H., Yu, Y., Safrina, O., Penna, A., Roos, J., Stauderman, K. A. and Cahalan, M. D. (2006). Genome-wide RNAi screen of Ca<sup>2+</sup>-influx identifies genes that regulate Ca<sup>2+</sup> release-activated Ca<sup>2+</sup> channel activity. *Proc. Natl. Acad. Sci. USA* **103**, 9357-9362.